Impact of Pigment Dispersion on Trabecular Meshwork Cells

Chao Wang,[1,2] Yalong Dang,[1] Ralitsa T. Loewen,[1] Susannah Waxman,[1] Priyal Shah,[1] Xiaobo Xia,[2*] Nils A. Loewen[1*]

1: Department of Ophthalmology, University of Pittsburgh Medical Center, Pittsburgh, Pennsylvania, United States

2: Department of Ophthalmology, Xiangya Hospital, Central South University, Changsha, Hunan, China.

*: Corresponding author

Abstract

Purpose: To investigate the effect of pigment dispersion on trabecular meshwork (TM) cells.

Methods: Porcine TM cells from ab interno trabeculectomy specimens were exposed to pigment dispersion, then analyzed for changes in morphology, immunostaining, and ultrastructure. Their abilities to phagocytose, migrate, and contract were quantified. An expression microarray, using 23,937 probes, and a pathway analysis were performed.

Results: TM cells readily phagocytosed pigment granules. Pigment induced stress fiber formation (pigment (P): 60.1 ± 0.3%, n=10, control (C): 38.4 ± 2.5%, n=11, $P<0.001$) and contraction at 24 hours onward ($P<0.01$). Phagocytosis declined (P: 68.7 ± 1.3%, C: 37.0 ± 1.1%, n=3, $P<0.001$) and migration was reduced after 6 hours (P: 28.0.1 ± 2.3, n=12, C: 40.6 ± 3.3, n=13, $P<0.01$). Microarray analysis revealed that Rho, IGF-1, and TGF β signaling cascades were central to these responses.

Conclusions: TM cell exposure to pigment dispersion resulted in reduced phagocytosis and migration, as well as increased stress fiber formation and cell contraction. The Rho signaling pathway played a central and early role, suggesting that its inhibitors could be used as a specific intervention in treatment of pigment glaucoma.

Introduction

Reduced outflow at the level of the trabecular meshwork (TM) is a principal cause of elevated intraocular pressure (IOP) in open-angle glaucomas.[1,2] Pigment dispersion has been reported to result in pigmentary glaucoma (PG), a form of secondary open-angle glaucoma, in 10% of patients after five years.[3,4] Medical treatment of PG is often more challenging than other glaucomas, and patients can exhibit high, fluctuating IOP.[5,6] Pigment released from the iris has been observed to accumulate in the TM, thereby increasing the IOP; however, the mechanism for this process is not well-understood. There is an insufficient quantity of pigment in the TM to cause a simple physical outflow obstruction[7]; yet, relatively low amounts of pigment are able to induce a hypertensive phenotype in ex vivo perfusion cultures.[8,9] Additionally, microarray expression analysis suggests a central role for ROCK and IGF-1[8] in the onset of PG.

In the present in vitro study, we sought to separate the TM cells from potentially confounding perfusion system-related factors, including regional outflow differences,[10] while avoiding potentially confounding in vivo factors, including an immune response.[11] We characterized changes in the TM cytoskeleton, contraction, motility, adhesion, tight junctions, and phagocytosis, as well as pathways associated with these factors.[12–15] Specifically, we characterized changes in the Rho family of small GTPases (Rho, Rac, and Cdc42), which act to rearrange the actomyosin cytoskeleton.[16] Importantly, lysophosphatidic acid, an activator of Rho GTPase, can increase the formation of actin stress fibers[17] and reduce aqueous outflow facility by 37%; a ROCK inhibitor can reverse these effects.[17] Further, Rac GTPase can modulate the intercellular adherens junctions[18] that contribute to TM cell motility[19] and phagocytosis.[9] We hypothesized that iris pigment particles may act on Rho GTPases to cause formation of actin stress fibers, thereby reducing TM contraction, motility, and phagocytosis.

Materials and Methods

Primary culture and characterization of porcine trabecular meshwork cells

Porcine eyes were obtained from a local abattoir (Thoma Meat Market, Saxonburg, PA) and processed within two hours of sacrifice. Extraocular tissues were carefully removed. After decontamination of globe exteriors in 5% povidone-iodine solution (3955-16, Ricca Chemical Company, Arlington, TX) for 3 minutes and three rinses with phosphate-buffered saline (PBS, 14190250, Thermo Fisher Scientific, Waltham, MA), TM tissues were carefully excised by ab interno trabeculectomy under a surgical microscope (S4, Carl Zeiss Meditec, Jena, Germany). The isolated TM tissues were then cut into 1-mm^3 fragments and cultured in Reduced Serum Media (Opti-MEM, 31985-070, Gibco, Life Technologies, Grand Island, NY), supplemented with 5% fetal bovine serum (FBS, 10438026, Thermo Fisher Scientific, Waltham, MA) and 1% antibiotic-antimycotic (15240062, Thermo Fisher Scientific, Waltham, MA). The medium was changed on day 7 and every 3 days thereafter. Cells were passaged after achieving 100% confluence. Only the first four passages of primary TM cells were used for this study.

TM cells were immunostained to validate their identity. Cell monolayers were fixed in 4% PFA for 1 hour and washed three times with PBS. Goat polyclonal anti-MGP (1:100, sc-32820, Santa Cruz, Dallas, Texas), rabbit polyclonal anti-alpha-SMA (1:100, ab5694, Abcam, Cambridge, MA) and anti-AQP1 (1:100, sc-20810, Santa Cruz, Dallas, Texas) antibodies were incubated overnight with the monolayers at 4°C. After washing three times with PBS, donkey anti-goat Alexa Fluor® 647 (1:1000, ab150131, Abcam, Cambridge, MA) and goat anti-rabbit IgG Superclonal™ (1:1000, A27034, Thermo Fisher Scientific, Waltham, MA) secondary antibodies were incubated with the samples at room temperature for 45 minutes. Cells incubated with PBS, instead of primary antibodies, served as a negative control condition. DAPI (D1306, Thermo Fisher Scientific, Waltham, MA) was added to the samples for 5 minutes to stain nuclei. Images were obtained with an upright laser scanning confocal microscope at 400-fold magnification (BX61, Olympus, Tokyo, Japan).

Induction of myocilin (MYOC), using dexamethasone, was used to confirm typical TM cell behavior. Briefly, cells at 50% confluence were exposed to 500 nM dexamethasone for 7 days. Cells cultured without dexamethasone-containing media served as the control condition. Cells were lysed in TriZol reagent (15596026, Invitrogen, Thermo Fisher, Waltham, MA), whole RNA was extracted, and a cDNA library was established using a reverse-transcription kit (4368814, Thermo Fisher Scientific, Waltham, MA). Following the manufacturer's instructions, quantitative PCR was performed on a Real-Time PCR System (4376600, Thermo Fisher Scientific, Waltham, MA). The primers used in the study were as follows: MYOC: sense: GGTCATTCCGGCAGTGAAGAA, antisense: ACGCCGTACTTGCCAGTGATT; GAPDH: sense: CCCCACCACACTGAATCTCC, antisense: GGTACTTTATTGATGGTACATGACAAG.

Preparation of pigment suspension

Irises of 10 porcine eyes were isolated and frozen at –80°C for 2 hours, then thawed at room temperature for 2 hours. This process was repeated twice to release pigment granules from lysed cells of the pigment epithelial layer. A total of 15 mL PBS was added to the suspension, and a 3-mL transfer pipette (13-711-20, Fisher Scientific) was used to promote further pigment release through 20 cycles of aspiration and

expulsion. The suspension was filtered through a 70-µm cell strainer (431751, Corning Incorporated, Durham, NC). The pigment suspension was diluted to 15 mL with PBS, then spun at 3000 rpm for 20 minutes; this step was repeated twice. The supernatant was discarded, and the pellet containing the isolated pigment was re-suspended in 4 mL PBS for use as a stock solution. The stock solution was diluted 1000-fold to count pigment particles on a hemocytometer, using 600 magnification (Eclipse TE200-E, Nikon Instruments Inc., Melville, NY), to determine their concentration.

Actin cytoskeleton

TM cells were seeded at a concentration of 1×105 cells/well into a 6-well plate atop cover glasses (2855-18, Corning Incorporated, Durham, NC) placed at the bottom of each well. After pigment dispersion (P) or control vehicle (C) for 7.5 days, cells were fixed with 4% PFA for 1 hour and washed three times with PBS. Coverslips were removed from their wells and incubated with DAPI for 5 minutes to label nuclei, and with Alexa Fluor 488 Phalloidin (1:60 dilution, A12379, Thermo Fisher, Waltham, MA) for 30 minutes to label F-actin. Cells were washed with PBS and twenty pictures from each experimental group were taken under an upright laser scanning confocal microscope (BX61, Olympus, Tokyo, Japan). Cells with stress fibers were counted.

Phagocytic activity assay

Primary TM cells were seeded at a density of 1×10^5 cells/well into a 6-well plate (657160, Greiner Bio-One, Frickenhausen, Germany). Three wells were exposed to pigment dispersion (P) at a concentration of 1.67×10^7 granules/mL for 24 hours, and three wells served as the pigment-free control (C). To assess phagocytosis, cells were incubated with FITC-labeled microspheres (F8813, Thermo Fisher, Waltham, MA), at a concentration of 5×10^8 microspheres/mL, for 1 hour. Monolayers were thoroughly washed three times with pre-warmed PBS, then cells were dissociated with trypsin and filtered with a 70-µm cell strainer. A single-cell suspension was made, and the percentages of fluorescent TM cells were measured by fluorescence-activated cell sorting (FACS). TM cells not incubated with microspheres served as a control condition.

Cell contraction assay

A cell contraction assay (CBA-201, Cell Biolabs, San Diego, CA, USA) was conducted according to the manufacturer's instructions, with minor modifications. In brief, a total of 1×10^6 cells were seeded into each of four T-75 flasks and maintained in TM medium. Pigment was added to one flask at a final concentration of 1.67×10^7 granules/mL, while the three control flasks were sham-treated with an equal volume of PBS. The medium was changed every 3 days. After 7.5 days, cells were trypsinized and resuspended in media. Collagen type I solution (3.0 mg/mL) was diluted in DMEM to a concentration of 1.9 mg/mL. Neutralized collagen type I solution was mixed with suspensions of TM cells at a final cell density of 6×10^5 cells/mL; mixing was performed on ice. A total of 125 µL of the cell-collagen mixture was added to each well of a 96-well plate (3596, Corning Incorporated, Durham, NC) and the mixtures were incubated at 37°C for 1 hour to allow gel formation. After gels had polymerized, 100 µL of TM cell media was added to each well, and the cell-collagen mixture was incubated at 37°C for 2 days. After incubation, 30-gauge needles were used to gently detach the gels from the inner walls of each well to initiate contraction. The gels were imaged at 0, 24, and 48 hours post-release. The size of the gels was measured using ImageJ software

(Version 1.50i, National Institutes of Health). Before gel detachment, the cells which were treated with the contraction inhibitor, 10 mM 2,3-Butanedione Monoxime (BDM) (CBA-201, Cell Biolabs, San Diego, CA, USA) served as a negative control, while the cells which were treated with a contraction promoter, 50 µM pilocarpine (61314020415, Sandoz, San Francisco, CA) served as a positive control.

Cell motility assay

TM cells were seeded into a 6-well plate at 3×10^5 cells/well and incubated at 37°C in TM medium, according to our previously published protocol.[20] After cells reached confluency, they were treated with 10 µg/mL Mitomycin (M4287, Sigma Aldrich) for 1 hour. Cells were washed with PBS three times, and new prewarmed TM media was added to the wells. A cell-free gap was created in the monolayer using a 10-µL sterile pipette tip (F1732031, Gilson, Middleton, WI). Detached cells were gently washed away by a combination of gentle plate agitation of the plate and three exchanges of prewarmed TM media. For cells in the P group, pigment granules were added into each well at a concentration of 1.67×10^7 granules/mL, while cells in the C group received an equal volume of PBS vehicle. Cells were cultured in a microscope stage incubator (H301-TC1-HMTC, Okolab, S.r.L., Ottaviano, NA, Italy), and pictures were taken at 40 magnification, every 6 hours for a total of 48 hours, using a live cell microscope system (Nikon Eclipse TI-E, Nikon, Tokyo, Japan). The cells infiltrating the wound area in each visual field were counted in ImageJ.

Cell adhesion assay

We also quantified cell-matrix adhesion. TM cells were seeded into a 6-well plate at 1×10^5 cells/well and incubated at 37°C in TM medium. After 7.5 days of exposure to pigment dispersion (P) or pigment-free control (C), confluent TM monolayers were washed by PBS for three times and 300 µl trypsin was added to each well. After 5 minutes trypsinization, TM cells were fixed with 4% PFA for 10 minutes and washed with PBS gently to remove the floating cells. The images were taken by a phase-contrast microscope at 200x magnification. The cells adhering on the well bottom in each visual area were counted by ImageJ.

H&E staining and transmission electron microscopy

Hematoxylin and eosin (H&E)-stained monolayers were utilized for gross histological evaluation. Pictures of samples were acquired under a SPOT microscope (BX60, Olympus, Tokyo, Japan) at 400 magnification. To observe finer changes in cellular ultrastructure, transmission electron microscopy (TEM) was used. TEM sample preparation followed a previous protocol[21], with minor modifications. Briefly, samples were fixed for 24 hours using 2.5% glutaraldehyde in 0.05 M cacodylate buffer, then washed with PBS three times. Samples were fixed overnight in a 1% osmium tetroxide solution. After washing with PBS three times, samples were dehydrated in an ascending ethanol series (30%, 50%, 70%, 90% and 100% ethanol, 45-minute incubations in each solution), and embedded in epon resin (Energy Beam Sciences, East Granby, CT). Epon was exchanged every hour for 3 hours and blocks were cured for 2 days at 60°C. A microtome (Reichert-Jung Ultracut 701701 Ultra Microtome) was used to cut 300-nm sections that were stained with a 0.5% Toluidine Blue O Solution (S25613, Thermo Fisher Scientific, Waltham, MA) to find areas of interest on bright-field microscopy. Ultrathin sections (65-nm thickness) were then obtained, placed on grids, and stained with uranyl acetate and lead citrate. Pictures were taken under an 80 kV Jeol transmission electron microscope (Peabody, The Jeol Legacy, MA) at 20,000 magnification.

Gene microarray

For the P group, TM cells were seeded into 60-mm dishes at 8×10^5 cells per dish (n=3 per group) using TM media supplemented with 1.67×10^7 pigment granules/mL, while cells in the C group were treated with an equal volume of PBS. After 7.5 days, cells were lysed with Trizol Reagent. The lysates were processed at the Genomic Core Facility of the University of Pittsburgh to ensure quality control. RNA extraction followed our previous protocol[22] and RNA purity was measured with a spectrophotometer (ND-2000, Fisher Scientific, Waltham, MA). For amplification and hybridization, we utilized an Affymetrix Porcine 3'IVT Array, which contains 23,937 probe sets to investigate 23,256 transcripts in pig, representing 20,201 Sus scrofa genes. The Affymetrix CEL files were loaded and normalized by Transcriptome Analysis Console (TAC) (Version 3.1, Affymetrix, Santa Clara, CA). Differential gene expression profiles were determined by applying a threshold of >1.5-fold linear change, with a p-value of <0.05. Genes that met the above criteria were mapped by bioinformatic pathway analysis software (Ingenuity Pathway Analysis, Qiagen, Hilden, Germany).

Statistics

All quantitative results were represented as mean ± standard error (SE). Differential gene expression and other quantitative data were processed by TAC and PASW 18.0 (SPSS Inc., Chicago, IL, USA) using one-way ANOVA, respectively. A p-value $\leq$0.05 was considered statistically significant.

Results

Characterization of primary porcine TM cells

After culture of freshly dissected TM, primary TM cells migrated into the flask and formed clones. These cells exhibited an even, polygonal shape different from the elongated shape of fibroblasts. As we previously reported,[8] primary TM cells became larger after 4–6 passages, indicative of a change in TM cell behavior. Because of this, our experiments only included TM cells that had undergone four or fewer passages. These cells stained positively for the TM markers alpha-SMA (Figure 1B), AQP1 (Figure 1C) and MGP (Figure 1D). Compared with the normal TM control, transcription of the MYOC gene was upregulated 1.5-fold after cells were incubated in 500 nM dexamethasone for 7.5 days. Our TM cells readily phagocytosed fluorescent microspheres.

Exposure to pigmented iris debris at a concentration of 1.67×10^7 granules/mL, resulted in considerable morphological changes in TM cells, which gradually gained an elongated and polygonal appearance within 1 week (Figure 1E, F, G, J). H&E staining revealed that most of the phagocytosed pigment particles were localized near the nucleus (Figure 1J). TEM demonstrated activation of lysosomes and phagosomes in the pigment group. Many pigment particles were ingested and were found in different stages of the lysosomal pathway, including hydrolysis by secondary lysosomes (Figure 1L). No pigment granules were found in the control TM culture (Figure 1K).

Morphological and functional changes

Pigment dispersion with a particle concentration of $1.67\text{x }10^7$ granules/mL caused TM cells to gradually take on an elongated and polygonal shape (Figure 1E, F, G, J). H&E staining revealed that most of the phagocytosed pigment particles were localized around the nucleus (Figure 1J, red arrows). Some

contraction of cell bodies was observed (Figure 1F, G, H, J, green arrows). TEM indicated the activation of lysosomes and phagosomes in the pigment-exposed TM cells. Many pigment particles were in different stages of being hydrolyzed by secondary lysosomes (Figure 1L).

F-actin stress fibers labeled with Alexa Fluor 488 Phalloidin in normal primary TM had a normal organization and the actin filaments were smooth and thin (Figure 2A, red arrows). After 24h of exposure to pigment dispersion, labeling showed thick, long, and curved stress fibers (Figure 2B, yellow arrows). The percentage of cells with stress fibers in P (60.1±0.3%, n=10 frames) was significantly higher than in controls (38.4±2.5%, n=11 frames, P<0.001).

TM phagocytosis of fluorescent microspheres quantified by FACS showed that pigment dispersion reduced the phagocytosis by 46.1% within 1 day (68.7±1.3% in the pigment group versus 37.0±1.1% in the control, P<0.001, Figure 3). TM cell contractile ability declined after pigment exposure for 7.5 days. The change in gel area was calculated at 24h and 48h after gel detachment and was significantly lower in P than in C at 24h (P:55.2±1.1%, C:29.6±1.8%, n=5, P<0.01) and at 48h (P:49.6±0.9%, C:23.6±2.2%, n=5, P<0.01, Figure 4).

We also evaluated the effects of pigment on cell migration using a wound healing assay. The numbers of TM cells which migrated into the wounded area were quantified at the 6, 12, and 18 hours post exposure. The results showed significantly less TM cell migration in P at all three time points, compared with C ((C: 40.6±3.3)% versus (P: 28.0±2.3)%, P<0.01 at the 6 hours; (C: 65.7±4.2)% versus (P:46.5±3.1)%, P<0.01 at the 12 hours; and (C: 86.1±5.9)% versus (P: 62.2±4.3)%, P<0.01 at 18 hours, Figure 5). After 7.5 days, the adhesion was reduced by 28.0±5.2% compared to controls (p<0.01).

Activation of Rho signaling by IGF-1 and TGF beta after pigment exposure

Signal pathways that are related to cellular contraction, migration, phagocytosis, cytoskeletal function, and tight junctions were altered. A total of 24,123 porcine genes were analyzed, of which 262 were significantly upregulated (Figure 6A, red dots in volcano plot and Figure 6B, red lines in the heat map) and 631 were significantly down-regulated (Figure 7A, green dots in volcano plot in and Figure 6B, green lines in heat map) by >1.5-fold (P<0.05).

After exclusion of 224 porcine genes with unclear biological functions, 669 porcine genes were mapped with Ingenuity Pathway Analysis (IPA). There was a significantly different expression of transcripts from 15 pathways related to phagocytosis, motility, tight junctions, actin cytoskeleton, and extracellular matrix remodeling (Figure 7). The Rho pathway played a central role in the response to pigment exposure, in that Rho was activated via stimulation of secreted bioactive molecule receptors, like transforming growth factor (TGF) β and type 1 insulin-like growth factor receptor (IGF-1). Activation of the Rho pathway was linked with regulation of myosin light chain (MLC), which was predicted to increase actin stress fiber polymerization and focal adhesion formation. This alteration would likely cause increased cellular contraction and decreased cellular migration, as well as inhibition of phagocytic ability (Figure 8). IL-8, JAK-Stat, and endothelin-1 signal pathways were involved in regulating cellular migration, while tight junctions were concurrently altered by over-expression of occludin (OCLN) and claudin 3 (CLDN3).

Discussion

In PG, pigment particles and stromal debris are released due to posterior iris bowing and friction with lens zonules and ciliary processes.[3] A heavily-pigmented TM is a distinct clinical feature of pigmentary glaucoma eyes that, when removed, results in normalization of outflow.[23] Our previous studies in perfusion cultures match this pattern, revealing that a low concentration of iris pigment particles increased intraocular pressure by 75%, relative to baseline; however, the underlying cellular and intracellular mechanisms remained unclear.[8] In our current study, we found significant reductions in TM phagocytosis, motility, contraction, along with an increase in TM stress fiber formation. Consistent with our *ex vivo* findings, TGF-β, IGF-1, and ROCK signaling are the three predominant pathways involved in the aforementioned cellular processes.

The cytoskeleton is composed of actin microfilaments, intermediate filaments, and microtubules[24], which can all impact the aqueous outflow; this occurs through cell contraction, movement, adhesion, and phagocytosis.[25–27] Formation of actin stress fibers, as we observed, can cause TM cell contraction[28] and increased aqueous outflow resistance.[14] These stress fibers can be observed after cells have undergone dexamethasone[14] or oxidative stresses.[29] Conversely, knockdown of 14-3-3z[30] and posttranscriptional inhibition of Rho kinase, using either a micro-RNA[12] or the carboxamide Y-27632[19], decreases contraction and increases outflow. In our studies, pigment caused TM cells to contract.

Phagocytosis is another feature of TM that presumably maintains outflow homeostasis by ensuring that the outflow tract remains free of debris.[31,32] The present study confirms that TM cells can phagocytose new debris within hours, beginning active breakdown in phagosomes and lysosomes, and that this process can become saturated relatively quickly. Our prior study found that a pigment-induced IOP elevation occurred prior to a decline in phagocytosis,[9] indicating that outflow-impacting cytoskeletal changes may occur even earlier. Like phagocytosis and contraction, TM cell migration declined within hours of pigment exposure, similar to the inhibitory effect of glucocorticoids[33], which also results in an elevation of IOP.[34] This effect can be countered by use of a Rho-kinase inhibitor.[19] Interestingly, Gottanka et al.[7] observed shortening of the inner wall of Schlemm's canal in PG that resulted in a partial (65%) lumen obstruction.

Consistent with our *ex vivo* perfusion findings, this signal pathway analysis also showed that activation of the Rho signaling pathway, through TGF β and IGF-1, played a central role in the responses that are triggered by pigment exposure. A TGF β-mediated activation of RhoA has also been described in primary open-angle glaucoma (POAG).[35,36] Elevation of IGF-1 can result in ocular neovascularization,[37] extracellular matrix (ECM) remodeling[38] and Rho pathway activation.[39] Conversely, inhibition of Rho signaling can result in reduced cell contraction and decreased IOP.[12,40,41] Taken together, these data suggest that rho-kinase inhibitors, which are currently in preclinical trials[42,43], may have potential to address the early mechanism of PG pathogenesis.

In conclusion, we investigated the impact of pigment dispersion on the primary trabecular meshwork. We found decreases in phagocytosis and cell migration, along with increases in cell contraction and stress fiber formation. A pathway analysis of pigment dispersion-related gene expression indicated a central role for Rho.

Acknowledgement

We acknowledge support from K08 K08-EY022737, from NIH CORE Grant P30 EY08098 to the Department of Ophthalmology, from the Initiative to Cure Glaucoma of the Eye and Ear Foundation of Pittsburgh, and from an unrestricted grant from Research to Prevent Blindness, New York, NY, an unrestricted grant from the Third Xiangya Hospital of Central South University for studying at the University of Pittsburgh (CW). We thank Ryan Chastain-Gross, Ph.D., from Liwen Bianji, Edanz Group China (www.liwenbianji.cn/ac), for editing the English text of a draft of this manuscript.

References

1. Goel M, Picciani RG, Lee RK, Bhattacharya SK. Aqueous humor dynamics: a review. *Open Ophthalmol J*. 2010;4:52-59.

2. Stamer WD, Braakman ST, Zhou EH, et al. Biomechanics of Schlemm's canal endothelium and intraocular pressure reduction. *Prog Retin Eye Res*. 2015;44:86-98.

3. Niyadurupola N, Broadway DC. Pigment dispersion syndrome and pigmentary glaucoma--a major review. *Clin Experiment Ophthalmol*. 2008;36(9):868-882.

4. Siddiqui Y, Ten Hulzen RD, Cameron JD, Hodge DO, Johnson DH. What is the risk of developing pigmentary glaucoma from pigment dispersion syndrome? *Am J Ophthalmol*. 2003;135(6):794-799.

5. De Moraes CG, Susanna R Jr. Glaucomas: Pigment Dispersion Syndrome, Pigmentary Glaucoma, and Angle Recession Glaucoma. In: Giaconi JA, Law SK, Nouri-Mahdavi K, Coleman AL, Caprioli J, eds. *Pearls of Glaucoma Management*. Springer Berlin Heidelberg; 2016:419-430.

6. Niyadurupola N, Broadway DC. Pigment dispersion syndrome and pigmentary glaucoma - a major review. *Clin Experiment Ophthalmol*. 2008;36(9):868-882.

7. Gottanka J, Johnson DH, Grehn F, Lütjen-Drecoll E. Histologic findings in pigment dispersion syndrome and pigmentary glaucoma. *J Glaucoma*. 2006;15(2):142-151.

8. Dang Y, Waxman S, Wang C, Loewen RT, Sun M, Loewen N. A porcine ex vivo model of pigmentary glaucoma. *bioRxiv*. August 2017:118448. doi:10.1101/118448.

9. Dang Y, Waxman S, Wang C, Loewen RT, Loewen NA. Intraocular pressure elevation precedes a phagocytosis decline in a model of pigmentary glaucoma. *bioRxiv*. August 2017:175695. doi:10.1101/175695.

10. Loewen RT, Brown EN, Roy P, Schuman JS, Sigal IA, Loewen NA. Regionally Discrete Aqueous Humor Outflow Quantification Using Fluorescein Canalograms. *PLoS One*. 2016;11(3):e0151754.

11. Epstein DL, Freddo TF, Anderson PJ, Patterson MM, Bassett-Chu S. Experimental obstruction to aqueous outflow by pigment particles in living monkeys. *Invest Ophthalmol Vis Sci*. 1986;27(3):387-395.

12. Luna C, Li G, Huang J, et al. Regulation of trabecular meshwork cell contraction and intraocular pressure by miR-200c. *PLoS One*. 2012;7(12):e51688.

13. Nakajima E, Nakajima T, Minagawa Y, Shearer TR, Azuma M. Contribution of ROCK in contraction of trabecular meshwork: proposed mechanism for regulating aqueous outflow in monkey and human eyes. *J Pharm Sci*. 2005;94(4):701-708.

14. Clark AF, Brotchie D, Read AT, et al. Dexamethasone alters F-actin architecture and promotes cross-linked actin network formation in human trabecular meshwork tissue. *Cell Motil Cytoskeleton*. 2005;60(2):83-95.

15. Filla MS, Schwinn MK, Nosie AK, Clark RW, Peters DM. Dexamethasone-associated cross-linked actin network formation in human trabecular meshwork cells involves β 3 integrin signaling. *Invest Ophthalmol Vis Sci*. 2011;52(6):2952-2959.

16. Amano M, Nakayama M, Kaibuchi K. Rho-kinase/ROCK: A key regulator of the cytoskeleton and cell polarity. *Cytoskeleton* . 2010;67(9):545-554.

17. Mettu PS, Deng P-F, Misra UK, Gawdi G, Epstein DL, Rao PV. Role of lysophospholipid growth factors in the

modulation of aqueous humor outflow facility. *Invest Ophthalmol Vis Sci*. 2004;45(7):2263-2271.

18. Pattabiraman PP, Epstein DL, Rao PV. Regulation of Adherens Junctions in Trabecular Meshwork Cells by Rac GTPase and their influence on Intraocular Pressure. *J Ocul Biol Dis Infor*. 2013;1(1). doi:10.13188/2334-2838.1000002.

19. Koga T, Koga T, Awai M, Tsutsui J-I, Yue BYJT, Tanihara H. Rho-associated protein kinase inhibitor, Y-27632, induces alterations in adhesion, contraction and motility in cultured human trabecular meshwork cells. *Exp Eye Res*. 2006;82(3):362-370.

20. Wang G-Q, Dang Y-L, Huang Q, et al. In Vitro Evaluation of the Effects of Intraocular Lens Material on Lens Epithelial Cell Proliferation, Migration, and Transformation. *Curr Eye Res*. 2017;42(1):72-78.

21. Yun H, Lathrop KL, Yang E, et al. A laser-induced mouse model with long-term intraocular pressure elevation. *PLoS One*. 2014;9(9):e107446.

22. Dang Y, Wu W, Xu Y, et al. Effects of low-level laser irradiation on proliferation and functional protein expression in human RPE cells. *Lasers Med Sci*. September 2015. doi:10.1007/s10103-015-1809-3.

23. Akil H, Chopra V, Huang A, Loewen N, Noguchi J, Francis BA. Clinical results of ab interno trabeculotomy using the Trabectome in patients with pigmentary glaucoma compared to primary open angle glaucoma. *Clin Experiment Ophthalmol*. 2016;44(7):563-569.

24. Ampe C, Vandekerckhove J. Actin and Actin Filaments. In: *eLS*. John Wiley & Sons, Ltd; 2001.

25. Tian B, Gabelt BT, Geiger B, Kaufman PL. The role of the actomyosin system in regulating trabecular fluid outflow. *Exp Eye Res*. 2009;88(4):713-717.

26. Kaufman PL. Enhancing trabecular outflow by disrupting the actin cytoskeleton, increasing uveoscleral outflow with prostaglandins, and understanding the pathophysiology of presbyopia: interrogating Mother Nature: asking why, asking how, recognizing the signs, following the trail. *Exp Eye Res*. 2008;86(1):3-17.

27. Tian B, Geiger B, Epstein DL, Kaufman PL. Cytoskeletal involvement in the regulation of aqueous humor outflow. *Invest Ophthalmol Vis Sci*. 2000;41(3):619-623.

28. Murphy KC, Morgan JT, Wood JA, Sadeli A, Murphy CJ, Russell P. The formation of cortical actin arrays in human trabecular meshwork cells in response to cytoskeletal disruption. *Exp Cell Res*. 2014;328(1):164-171.

29. Zhou L, Li Y, Yue BY. Oxidative stress affects cytoskeletal structure and cell-matrix interactions in cells from an ocular tissue: the trabecular meshwork. *J Cell Physiol*. 1999;180(2):182-189.

30. Ye Y, Yang Y, Cai X, Liu L, Wu K, Yu M. Down-regulation of 14-3-3 Zeta Inhibits TGF-β 1–Induced Actomyosin Contraction in Human Trabecular Meshwork Cells Through RhoA Signaling Pathway14-3-3 Zeta Regulates Actomyosin Contraction in TM Cells. *Invest Ophthalmol Vis Sci*. 2016;57(2):719-730.

31. Gagen D, Filla MS, Clark R, Liton P, Peters DM. Activated αvβ3 integrin regulates αvβ5 integrin-mediated phagocytosis in trabecular meshwork cells. *Invest Ophthalmol Vis Sci*. 2013;54(7):5000-5011.

32. Zhang X, Ognibene CM, Clark AF, Yorio T. Dexamethasone inhibition of trabecular meshwork cell phagocytosis and its modulation by glucocorticoid receptor beta. *Exp Eye Res*. 2007;84(2):275-284.

33. Clark AF, Wilson K, McCartney MD, Miggans ST, Kunkle M, Howe W. Glucocorticoid-induced formation of cross-linked actin networks in cultured human trabecular meshwork cells. *Invest Ophthalmol Vis Sci*.

1994;35(1):281-294.

34. Mao W, Tovar-Vidales T, Yorio T, Wordinger RJ, Clark AF. Perfusion-cultured bovine anterior segments as an ex vivo model for studying glucocorticoid-induced ocular hypertension and glaucoma. *Invest Ophthalmol Vis Sci*. 2011;52(11):8068-8075.

35. Inatani M, Tanihara H, Katsuta H, Honjo M, Kido N, Honda Y. Transforming growth factor-beta 2 levels in aqueous humor of glaucomatous eyes. *Graefes Arch Clin Exp Ophthalmol*. 2001;239(2):109-113.

36. Fuchshofer R, Tamm ER. The role of TGF-β in the pathogenesis of primary open-angle glaucoma. *Cell Tissue Res*. 2012;347(1):279-290.

37. Smith LE, Shen W, Perruzzi C, et al. Regulation of vascular endothelial growth factor-dependent retinal neovascularization by insulin-like growth factor-1 receptor. *Nat Med*. 1999;5(12):1390-1395.

38. Kilani RT, Guilbert L, Lin X, Ghahary A. Keratinocyte conditioned medium abrogates the modulatory effects of IGF-1 and TGF-β 1 on collagenase expression in dermal fibroblasts. *Wound Repair Regen*. 2007;15(2):236-244.

39. Dogan AS, Kabatas N, Erden G, Celikay O, Arzuhal AE, Gurdal C. Serum insulin-like growth factor-1 levels in patients with pseudoexfoliation syndrome and glaucoma. *Int Ophthalmol*. 2017;37(2):371-375.

40. Ramachandran C, Patil RV, Sharif NA, Srinivas SP. Effect of elevated intracellular cAMP levels on actomyosin contraction in bovine trabecular meshwork cells. *Invest Ophthalmol Vis Sci*. 2011;52(3):1474-1485.

41. Pattabiraman PP, Inoue T, Rao PV. Elevated intraocular pressure induces Rho GTPase mediated contractile signaling in the trabecular meshwork. *Exp Eye Res*. 2015;136:29-33.

42. Inoue T, Tanihara H. Rho-associated kinase inhibitors: a novel glaucoma therapy. *Prog Retin Eye Res*. 2013;37:1-12.

43. Bacharach J, Dubiner HB, Levy B, Kopczynski CC, Novack GD, AR-13324-CS202 Study Group. Double-masked, randomized, dose-response study of AR-13324 versus latanoprost in patients with elevated intraocular pressure. *Ophthalmology*. 2015;122(2):302-307.

Figures

Figure 1

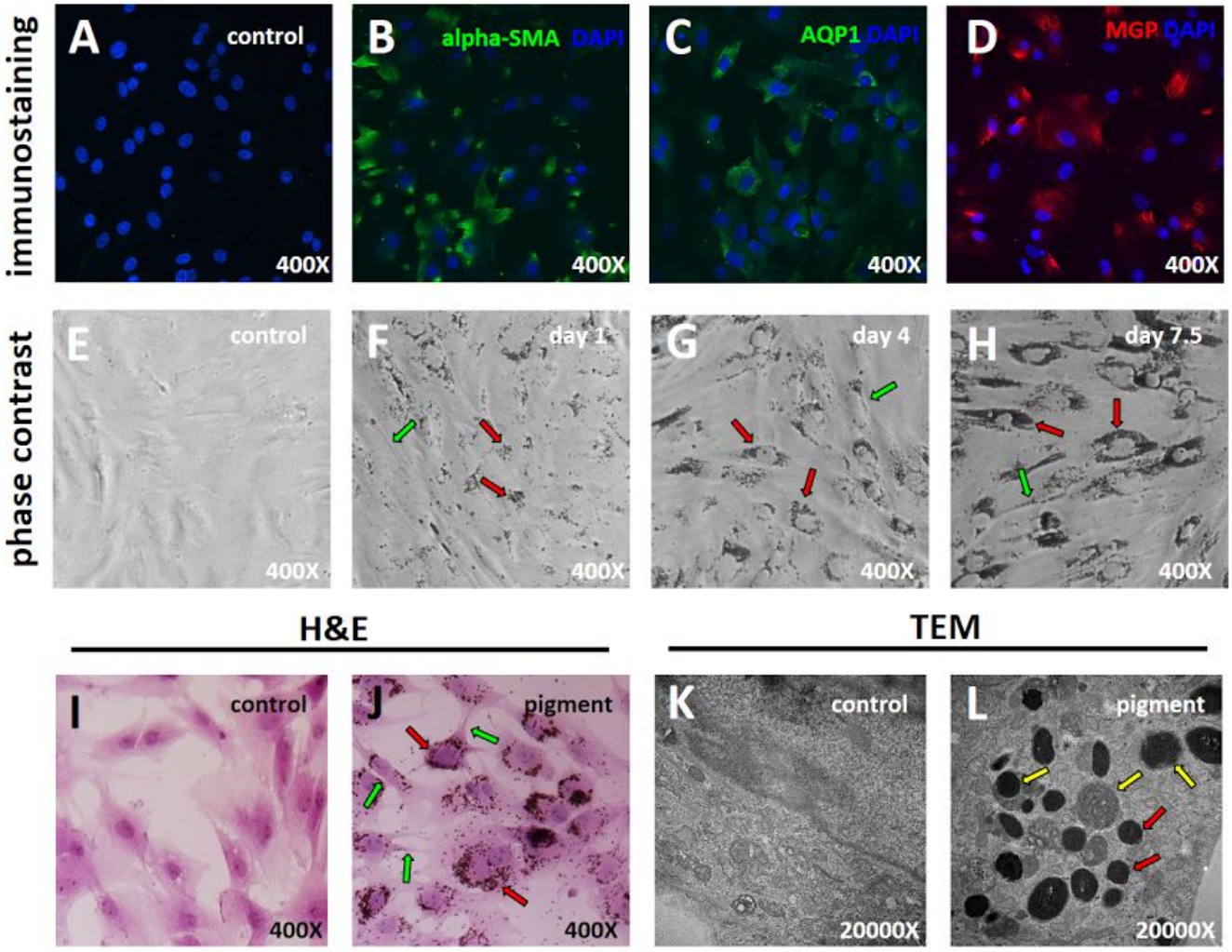

Figure 1. Primary trabecular meshwork (TM) cell characterization and pigment exposure. Probing with TM-specific markers alpha-SMA (Figure 1, B), AQP1 (Figure 1C) and MGP (Figure 1D) revealed positive staining for all markers. Phase-contrast imaging of TM cells after 1 day (Figure 1F, red arrows), 4 days (Figure 1G, red arrows) and 7.5 days (Figure 1H, red arrows) of pigment showed accumulation of pigment granules in the cytoplasm and around the cell nuclei. H&E staining of TM cells showed that the pigment granules were located within cells (Figure 1J, red arrows). Some contraction of cell bodies was observed (Figure 1F, G, H, J, green arrows). Transmission electron microscopy showed the ultrastructure of organelles (Figure 1K). In the control (C) group, there were no pigment granules within cells, but in the pigment dispersion group, abundant pigment granules were found in the cytoplasm (Figure 1L, red arrows). Some pigment granules were in different stages of phagolysosomal digestion (Figure 1L, yellow arrows).

Figure 2

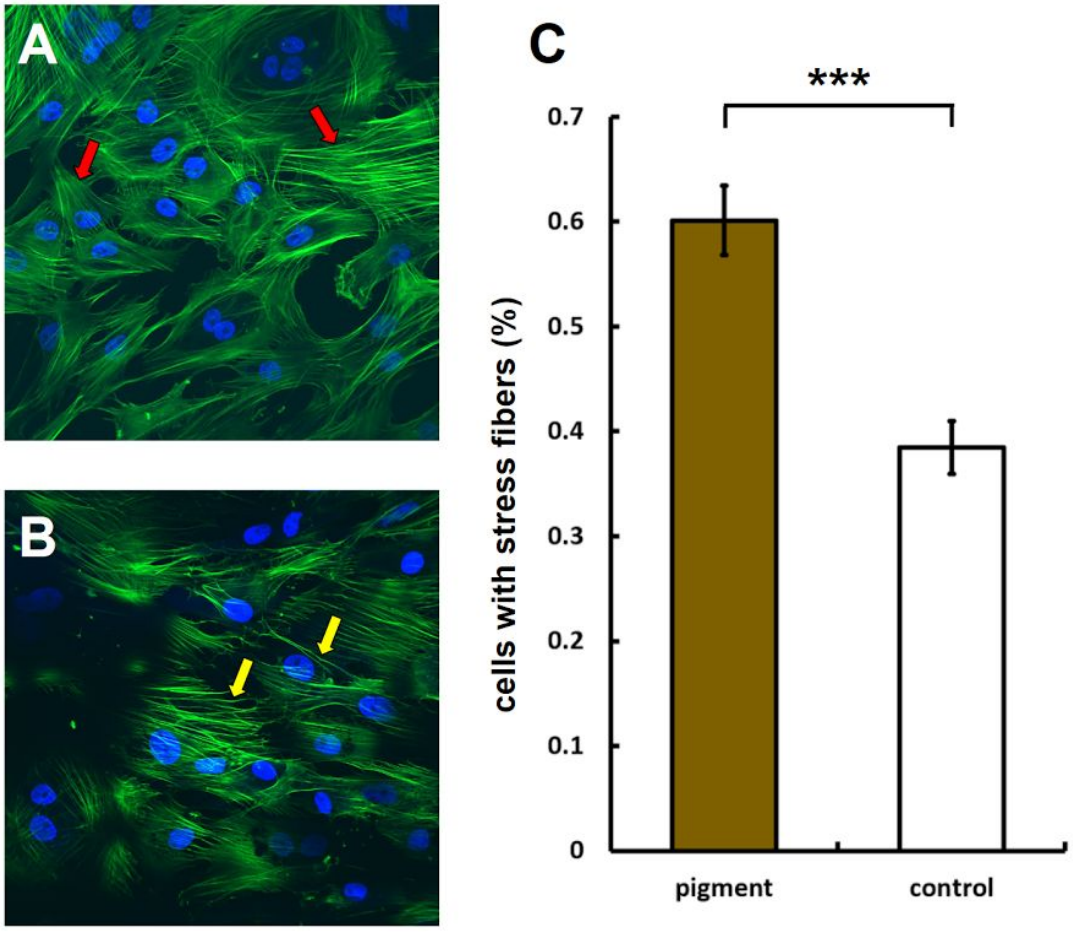

Figure 2. F-actin stress fibers formation. In the control group, trabecular meshwork (TM) cells exhibited smooth and thin F-actin filaments (Figure 2A, red arrows). After 24 hours, TM cells exhibited F-actin with thick, long, and curved stress fibers (Figure 2B, yellow arrows). The pigment dispersion group (60.1 ± 0.3%, n=10) contained a significantly larger number of cells with stress fibers, compared to the control group (38.4 ± 2.5%, n=11, ***P<0.001; Figure 2C).

Figure 3

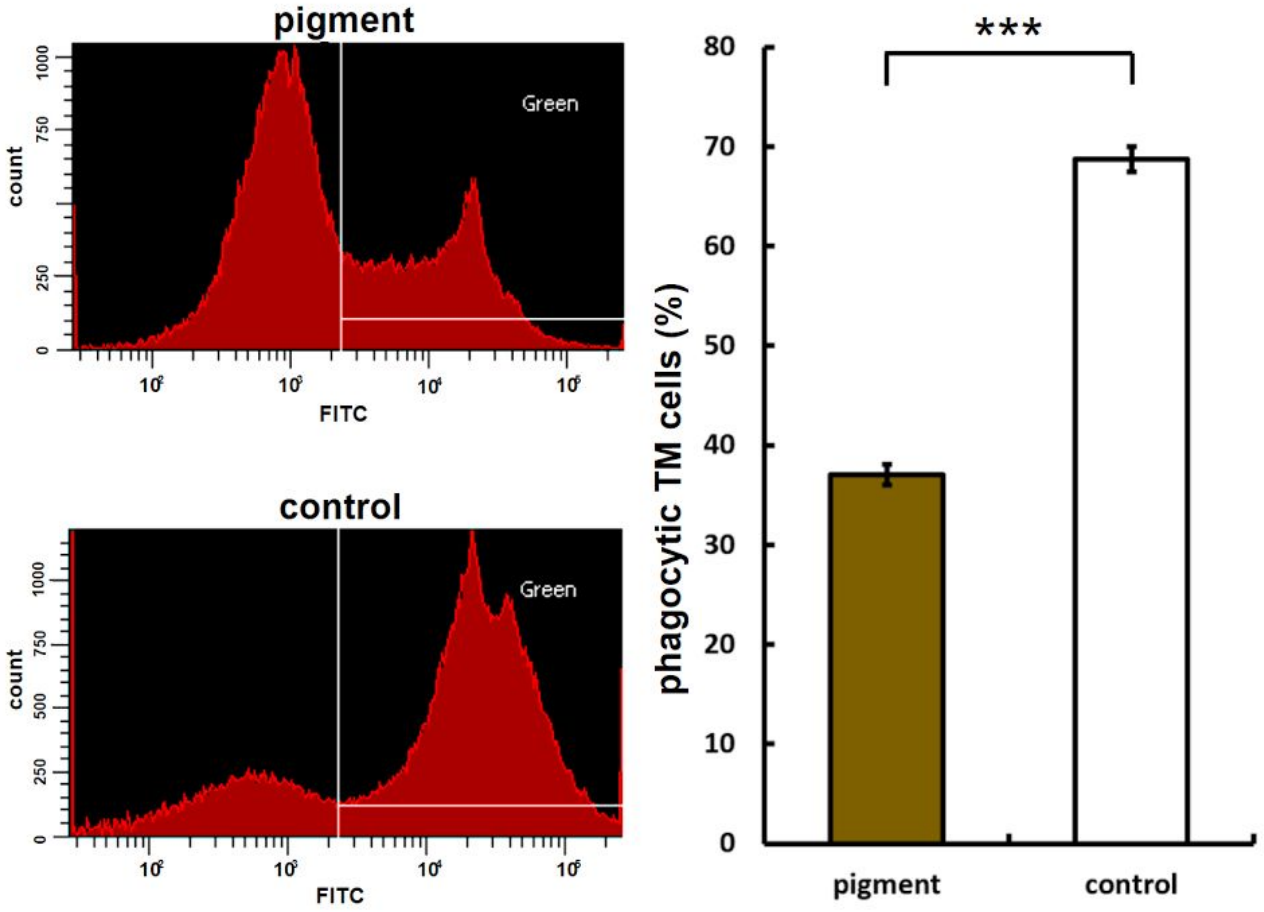

Figure 3. Reduced phagocytosis. Uptake of yellow-green fluorescent microspheres in the pigment dispersion group was significantly lower (37.0 ± 1.1%) than uptake in the control group (C, 68.7 ± 1.3%, n=3, ***P<0.001)

Figure 4

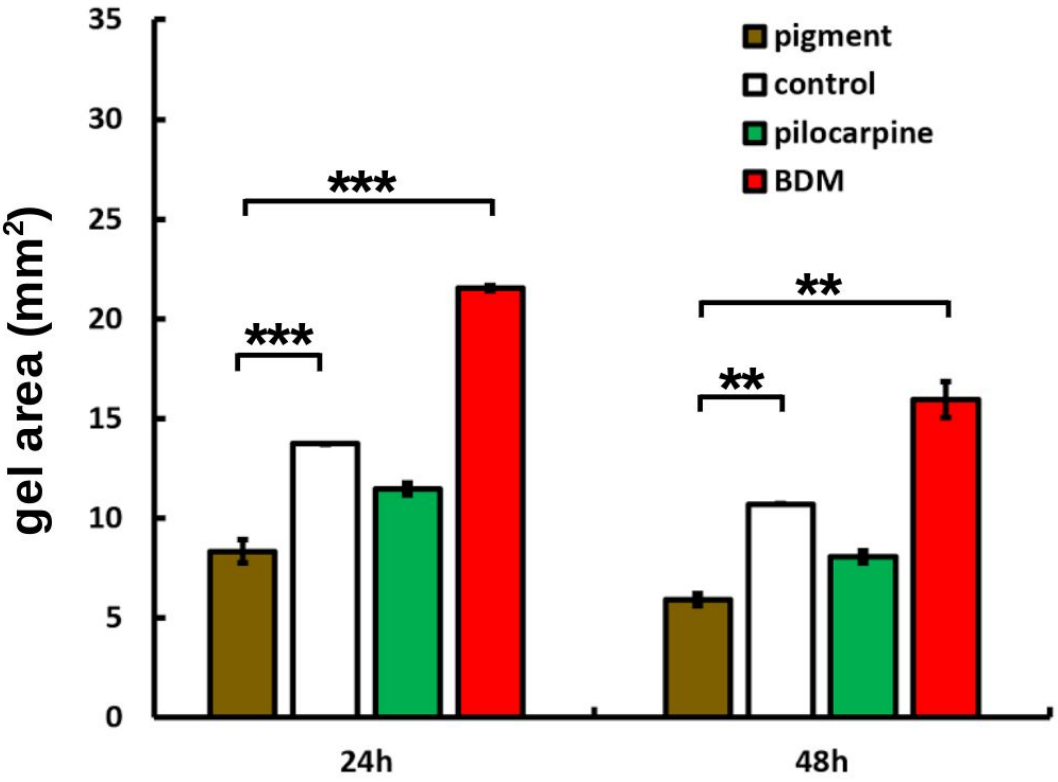

Figure 4. TM cell contraction. Gel contraction is shown at 24 and 48 hours post detachment from a baseline of 30 mm^2. Pigment contracted the most followed by pilocarpine, the control, and contraction inhibitor 2,3-Butanedione monoxime (BDM). Gel area in the pigment-treated group (P) were significantly smaller than gel size in the control group (C) at 24 hours (P: 8.3 ± 0.6 mm^2, C: 13.6 ± 0.0 mm^2, n=2, ***P<0.001) and at 48 hours (P: 5.9 ± 0.3 mm^2, C: 10.7 ± 0.0%, n=2, **P<0.01, Figure 4).

Figure 5

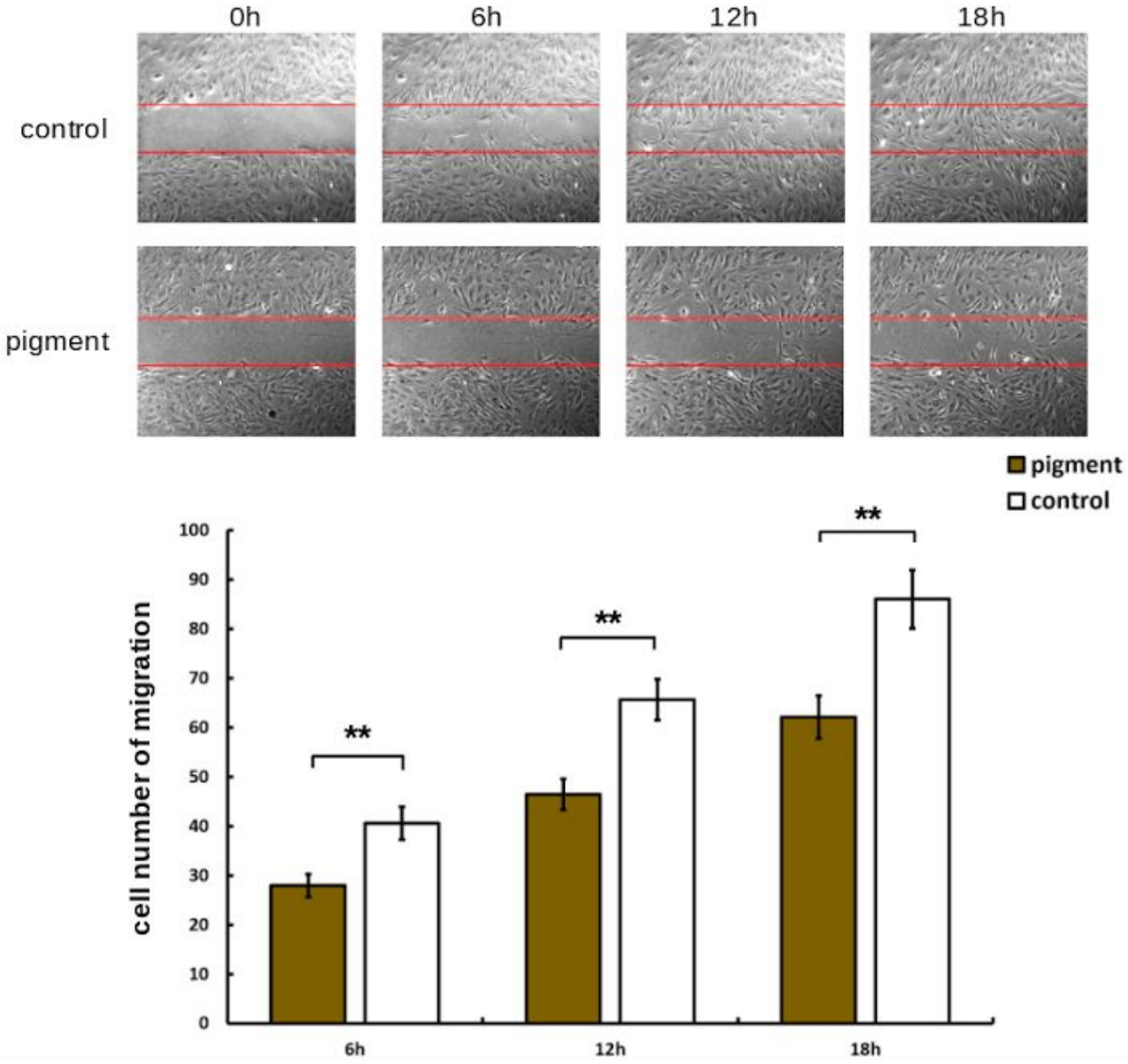

Figure 5. Reduced cell migration. Top panels show representative phase-contrast images of the control group (C) at 0–18 hours after wounding. Bottom panels show the pigment-dispersion group (P) at the same time points. Bar chart reveals that cell migration into the denuded area is significantly higher in C than in P at 6 hours (Figure 4, C: 40.6 ± 3.3, P: 28.0.1 ± 2.3, **P<0.01), 12 hours (C: 65.7 ± 4.2, P: 46.5 ± 3.1, **P<0.01), and 18 hours (C: 86.1 ± 5.9, P: 62.2 ± 4.3, **P<0.01) (C: n= 13 frames per time point, P: n=12 frames per time point).

Figure 6

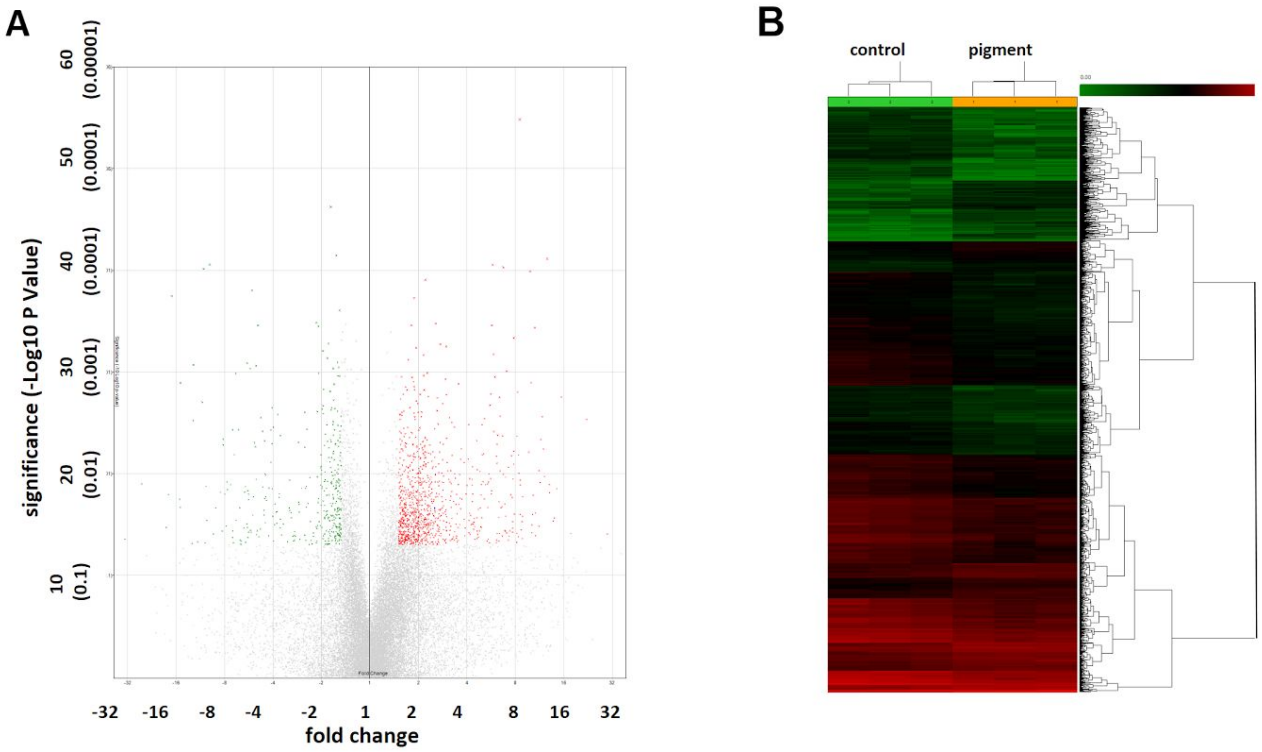

Figure 6. Gene expression changes. A total of 24,123 porcine genes were analyzed, of which 262 were significantly upregulated (red dots in volcano plot (Figure 6A) and red lines in heatmap (Figure 6B)) and 631 were significantly down-regulated (green dots in volcano plot in and green lines in heat map) by >1.5-fold, following pigment dispersion ($P<0.05$).

Figure 7

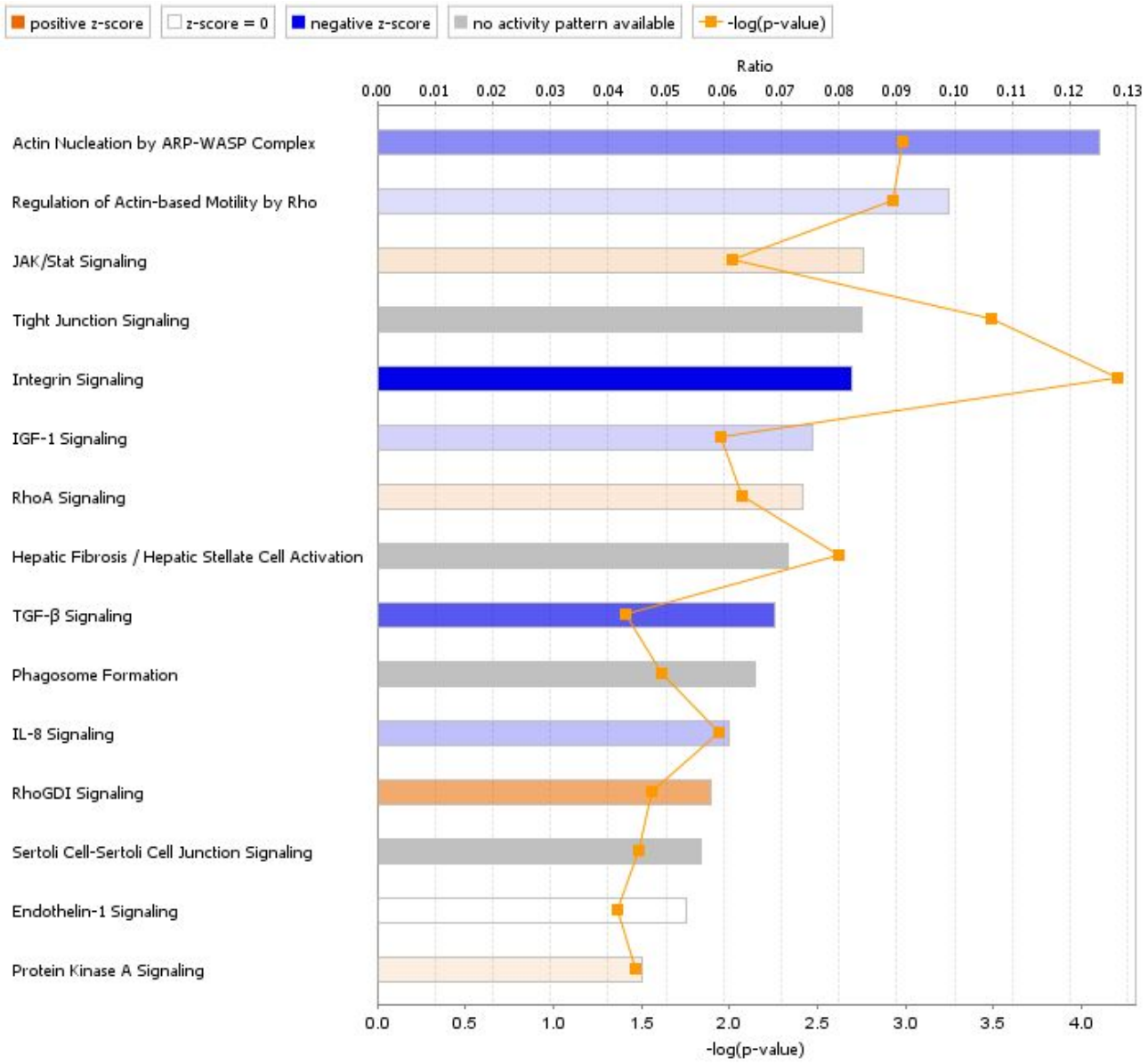

Figure 7. Signal pathway changes after pigment exposure. Regulation was significantly different in 15 signal transduction pathways related to phagocytosis, motility, tight junctions, actin cytoskeleton, and extracellular matrix remodeling. The z-score is a statistical measure of the match between expected relationship direction and observed gene expression.

Figure 8

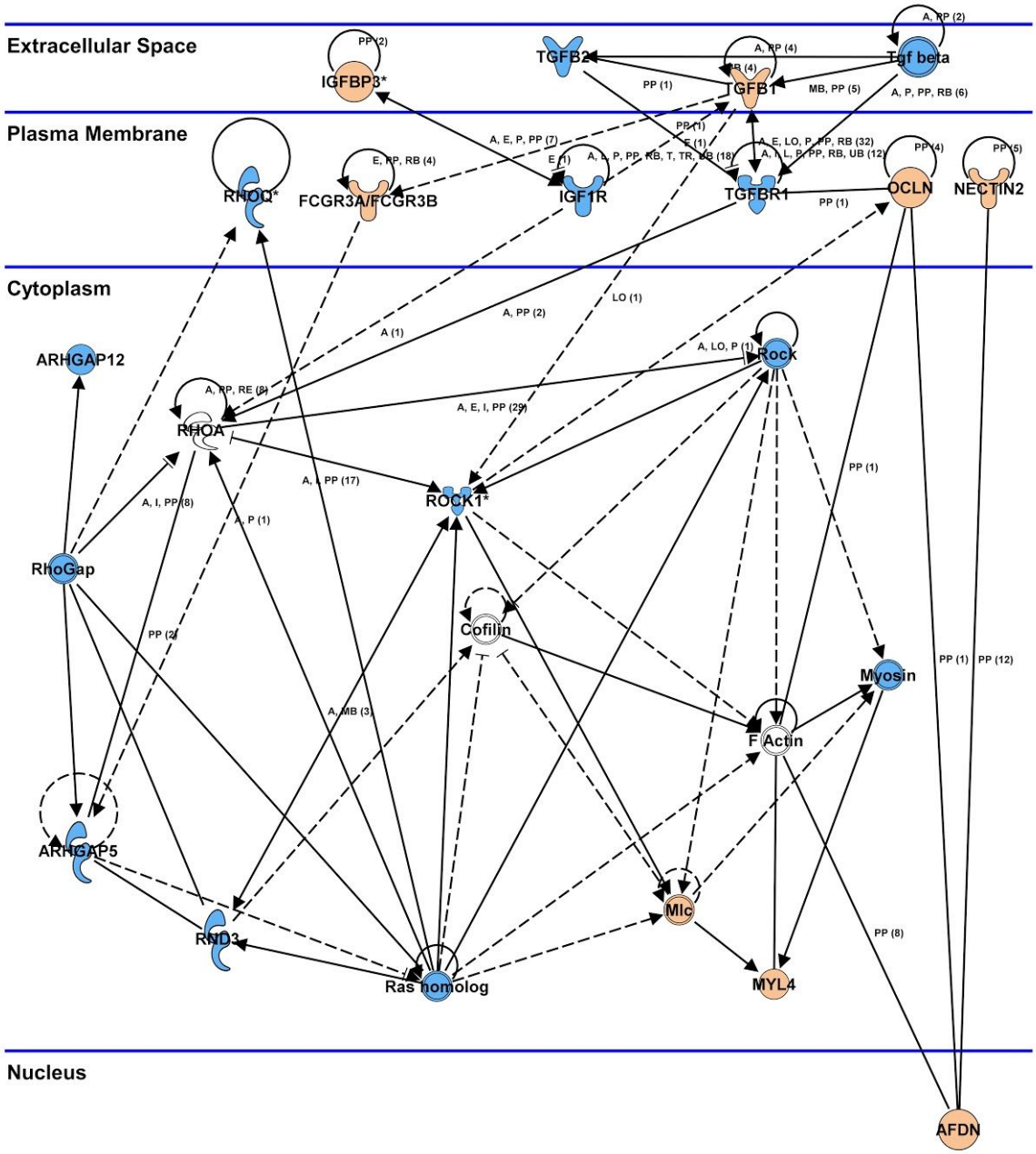

Figure 8. Network analysis. The Rho signaling pathway played a crucial role in the response to pigment exposure, and was activated via stimulation of TGF β and IGF-1. Activation of the Rho pathway resulted in MLC upregulation, which is predicted to lead to actin stress fiber polymerization and focal adhesion formation. This process would likely result in increased cellular contraction and decreased cellular migration, as well as inhibition of phagocytic ability. Key tight junction genes, including OCLN and CLDN3, were upregulated after pigment exposure. Orange: up-regulation, Blue: down-regulation.

Tables

Table 1. Expression changes in key genes and their pathways, following exposure to pigment

Gene Symbol	Entrez Gene Name	Fold Change	*P*-value (ANOVA)	Signal Pathways
OCLN	occludin	8.26	0.036	Tight junction signaling, Sertoli cell-sertoli cell junction signaling
FCGR3A/FCGR3B	Fc fragment of IgG receptor IIIa	5.07	0.039	Phagosome formation
ITGA4	integrin subunit alpha 4	4.12	0.007	RhoGDI signaling, actin nucleation by ARP-WASP complex, integrin signaling, regulation of actin-based motility by Rho, phagosome formation
IGFBP3	insulin like growth factor binding protein 3	3.73	0.003	IGF-1 signaling
CLDN3	claudin 3	2.76	0.024	Tight junction signaling, Sertoli cell-sertoli cell junction signaling
RHOB	ras homolog family member B	1.89	0.004	RhoGDI signaling, actin nucleation by ARP-WASP complex, integrin signaling, regulation of actin-based motility by Rho, IL-8 signaling, phagosome formation
MYL4	myosin light chain 4	1.87	0.023	RhoA signaling, RhoGDI signaling, regulation of actin-based motility by Rho, tight junction signaling, protein kinase A signaling
TGFB1	transforming growth factor beta 1	1.56	0.012	TGF-β signaling, tight junction signaling, protein kinase A signaling
TGFBR1	transforming growth factor beta receptor 1	-1.54	0.039	TGF-β signaling, tight junction signaling, protein kinase A signaling
IGF1R	insulin like growth factor 1 receptor	-1.56	0.037	RhoA signaling, IGF-1 signaling

RHOQ	ras homolog family member Q	-1.58	0.040	RhoGDI signaling, actin nucleation by ARP-WASP complex, integrin signaling, regulation of actin-based motility by Rho, IL-8 signaling, phagosome formation
ARHGAP12	Rho GTPase activating protein 12	-1.87	0.001	RhoGDI signaling, RhoA signaling
ITGB8	integrin subunit beta 8	-1.9	0.024	integrin signaling
ARHGAP5	Rho GTPase activating protein 5	-1.93	0.047	RhoGDI signaling, RhoA signaling, integrin signaling
ITGAV	integrin subunit alpha V	-1.96	0.018	IL-8 signaling, integrin signaling
TGFB2	transforming growth factor beta 2	-1.99	0.029	TGF-β signaling, tight junction signaling, protein kinase A signaling
ROCK1	Rho associated coiled-coil containing protein kinase 1	-2.1	0.009	RhoA signaling, actin nucleation by ARP-WASP complex, integrin signaling, regulation of actin-based motility by Rho, IL-8 signaling, protein kinase A signaling
ITGA1	integrin subunit alpha 1	-2.24	0.017	integrin signaling
IGFBP1	insulin like growth factor binding protein 1	-2.52	0.022	IGF-1 signaling
ITGA2	integrin subunit alpha 2	-2.55	0.010	RhoA signaling, actin nucleation by the ARP-WASP complex, integrin signaling, regulation of actin-based motility by Rho, phagosome formation
RND3	Rho family GTPase 3	-2.91	0.045	RhoA signaling, actin nucleation by ARP-WASP complex, integrin signaling, regulation of actin-based motility by Rho, phagosome formation, IL-8 signaling